THERMALLY INDUCED CHANGES OF THE CARBONATE STRUCTURE IN BIOLOGICAL HYDROXYAPATITE STUDIED BY EPR AND ENDOR

S.S. ISHCHENKO, I.P. VORONA, N.P. BARAN, S.M. OKULOV, V.V. RUDKO

Institute of Semicondictor Physics, Nat. Acad. of Sci. of Ukraine
(41, Nauky Prosp., Kyiv 03028, Ukraine; e-mail: ip_ vorona@yahoo.com)

UDC 539.219; 539.184

Changes of the carbonate structure in tooth enamel hydroxyapatite under annealing in the temperature interval T_{ann} = 20–1000 °C are studied by electron paramagnetic resonance (EPR) and electron nuclear double resonance (ENDOR). In our studies, CO_2^- radicals induced by γ-irradiation after the annealing of specimens are used as a probe. The lineshape of EPR spectra and proton (^{1}H) and phosphorus (^{31}P) ENDOR spectra, as well as their thermally induced modifications, are analyzed and explained. It is shown that the general tendency under the annealing of specimens is the escape of carbonate from biohydroxyapatites and its simultaneous transformation from type B into type A at $T_{ann} > 700$ °C. Specific features of carbonate escape from biohydroxyapatite at $T_{ann} = 400$ °C are explained by the formation of localized CO_2 molecules in apatite. The results obtained correlate with the data of IR and NMR studies of tooth enamel, as well as with the EPR and ENDOR spectra of CO_2^- radicals in synthetic hydroxyapatites.

1. Introduction

Biological hydroxyapatite (HAP) $Ca_{10}(PO_4)_6(OH)_2$ synthesized directly in alive organisms is the mineral base of biological tissues. It is present in various amounts in all organs of living beings and plays a significant role in the formation of properties of organisms, metabolism, ageing, and diseases. There are physiological HAP and pathogenic HAP. Physiological HAP is the mineral base of teeth (∼95%) and bones (∼65%), while pathogenic HAP is a part of gallstones, patches on walls of blood vessels, brain sand, etc. Knowledge of both the structure of biological HAP and its changes under the action of various factors opens a possibility to stimulate the physiological mineralization and to block the pathogenic one. In organisms, HAP is present in the form of nano-sized crystals (10-150 nm), the so-called crystallites. The crystallites are immersed in an aqueous-organic matrix, and the stability of their structure and composition is ensured by metabolism via this matrix.

The typical crystallochemical feature of biological HAP is the presence of carbonate. The content of carbonate can be as large as several per cents. The amount and the structure of these compounds in biological tissues reflect various pathologies of teeth and bones, the demineralization of tissues after a prolonged state of weightlessness, as well as the assimilation with implants [1, 2]. Carbonate is present in biocrystallites mainly in the form of CO_3^{2-} carbonate-ions which replace PO_4^{3-} anions (HAP of type B) or OH groups aligned along the sixth-order axis (HAP of type A) in the lattice of HAP. Ionizing radiation or ultraviolet (UV) light induces the formation of carbon radicals that cause the electron paramagnetic resonance (EPR) signal near $g = 2$. This signal has been studied in many papers (see, e.g., [3–5]) due to its numerous applications in retrospective EPR dosimetry [3, 6] and archeological dating [6–8]. It was shown [9–12] that the main contribution to the radiation-induced EPR signal in HAP is related to CO_2^- radicals of two types: CO_2^- radicals with axial symmetry and CO_2^- radicals with orthorhombic symmetry. Axial CO_2^- radicals freely rotate around the O–O axis, while the rotation of orthorhombic radicals is hampered by near-by defects in the lattice.

In spite of numerous previous studies, the following is still not clear: which species are the precursors of CO_2^- radicals, where are they located in the lattice, and which is the mechanism of their formation? For example, there is a suggestion that CO_2^- radicals in biological HAP are

formed from CO_2 molecules that are located near the surface of crystallites or in the organic part of tissue. However, in this case, CO_2 precursors and related CO_2^- radicals would be unstable, which contradicts [13, 14] and is in variance with the application of CO_2^- radicals in dosimetry and dating.

We believe that the main precursors of CO_2^- radicals in biological HAP are CO_3^{2-} carbonate-ions. Under ionizing radiation or UV light, the secondary electrons appear in HAP, and CO_3^{2-} are transformed into unstable CO_3^{3-}; the latter decay with the formation of CO_2^-. This mechanism is confirmed by optical [15] and NMR [16] measurements, as well as by our studies of EPR [17] and ENDOR [18]. Therefore, CO_2^- radicals can be used as structural probes in order to get information about the carbonate subsystem of HAP and its nearest surrounding.

As known [19], HAP in tooth enamel is predominantly the *B*-type HAP. Therefore, we assume hereafter that the carbon impurity in initial HAP is mainly represented by CO_3^{2-} carbonate ions in position *B*. The purpose of the present work is to study the changes of the carbonate structure of biological HAP under annealing in a wide temperature interval. We will analyze the EPR and ENDOR spectra of CO_2^- radicals formed in tooth enamel by γ-radiation after the annealing.

2. Materials and Methods

We studied powdered human tooth enamel. This allows us to avoid orientation-dependent variations of signals of magnetic resonances. In our studies, we used the enamel of sound teeth received from stomatological clinics. After the removal of dentin, the enamel was ground into a powder with the size of granules of 100–300 μm.

The isochronous annealing of specimens was performed in a muffle furnace in air at temperatures up to 1000 °C inclusively. The annealing duration was 60 min at each chosen temperature. The temperature was controlled with a thermocouple; the accuracy of measurements was ±1 °C. After the annealing, the specimens were irradiated with γ-rays from ^{60}Co, the exposure rate was 2.58×10^{-2} $\mathrm{Ckg^{-1}s^{-1}}$ (100 R/s). The absorbed dose was approximately 10^4 Gy. The measurements of EPR spectra were carried out in the 3-cm range by a Radiopan SE/X-2547 spectrometer at room temperature. The microwave power (∼5 mW) and the modulation amplitude of the magnetic field (0.2 mT) corresponded to the conditions that are most frequently used for analogous studies, in particular in EPR dosimetry. The ENDOR spectra were measured at the temperature $T = 4.2$ K with the use of a superheterodyne spectrometer EYa-1301. The spectra were registered at various values of magnetic field within the EPR line. The intensities of the studied EPR spectra were normalized by the intensity of the EPR signal from a reference MgO:Cr^{3+} specimen mounted in the cavity. This ensures the accuracy of measurements of the amplitude of spectra not worse than 1 % (in the presented figures, the error bars do not exceed the size of the experimental points).

For the modeling of the powder EPR spectra, we used a computer program developed by us; the components of *g*-tensor, as well as width and shape of the initial EPR line, were taken as input parameters. The intensities of components of the EPR spectrum were fitted using the Separator program from the Visual EPR package [20].

3. Experimental Results and Discussion

3.1. EPR studies

In the initial (nonirradiated) specimens of tooth enamel, EPR signals from carbonate radicals were not registered neither before nor after the annealing. We studied 11 specimens, each one was preliminarily annealed at a certain temperature T_{ann} in the interval (20–1000 °C) and then irradiated by γ-rays. After the irradiation, the well-known EPR spectrum near $g = 2$ appears [3]. This spectrum is a superposition of signals from various paramagnetic centers. As was shown in [10, 11], the dominating contribution to the spectra is caused by orthorhombic ($g_x = 2.0030$, $g_y = 2.0015$, $g_z = 1.9970$) and axial ($g_{||} = 1.9970$, $g_{\perp} = 2.0027$) CO_2^- radicals. We have fitted the EPR spectra of the annealed samples and demonstrated that, at any annealing temperature, the EPR spectrum of enamel can be described predominantly by the contributions of orthorhombic and axial CO_2^- radicals. In the fitting, we have neglected relatively weak signals of the unknown origin that contribute to the low-field wing of the EPR line. These signals give an inessential contribution to the central part of the total EPR signal and no contribution to its high-field part. The EPR spectra at the most characteristic temperature points are shown in Fig. 1. The ratio between orthorhombic and axial CO_2^- radicals was calculated by the method proposed in [12, 21]. This ratio was constant (in the limits of experimental errors, ±0.05) up to 250 °C and was equal to 4.00. At $T_{\mathrm{ann}} > 250$ °C, the EPR spectrum intensity decreased

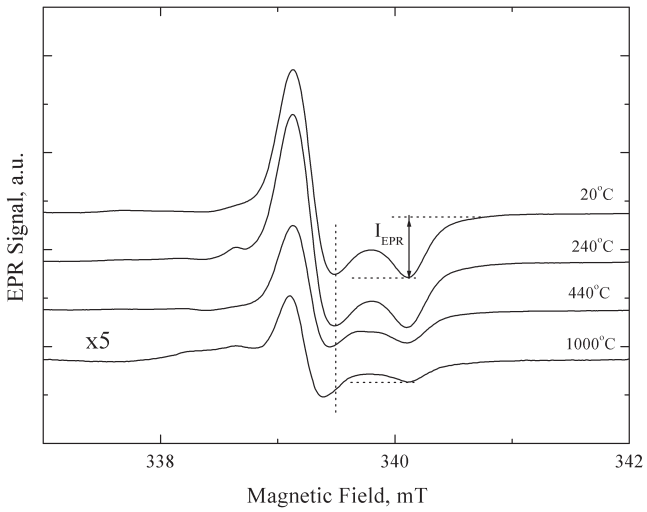

Fig. 1. EPR spectra of γ-irradiated specimens of tooth enamel that were annealed before the irradiation at the indicated temperatures

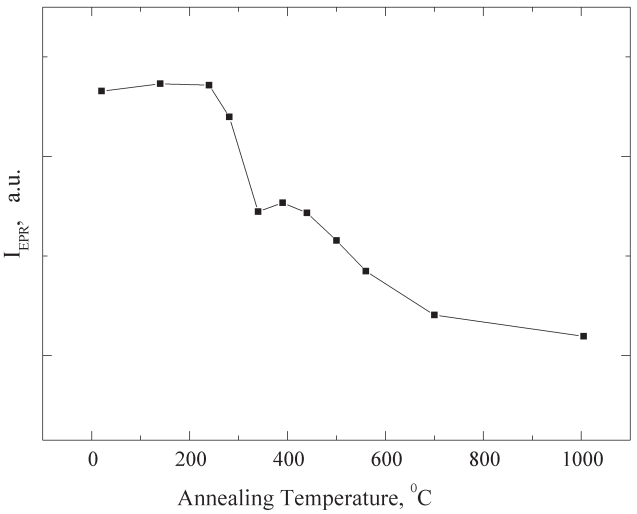

Fig. 2. Amplitude $I_{\rm EPR}$ versus the annealing temperature

due to a decrease of the total amount of CO_2^- radicals. In the same temperature interval, the relative contribution of orthorhombic centers decreased and, correspondingly, the EPR lineshape changed. Namely, the low-field minimum of the signal became deeper as compared with the high-field minimum and shifted to the low-field side (see Fig. 1). A comprehensive analysis of lineshape changes of γ-irradiated tooth enamel powder related to the change of the ratio of orthorhombic and axial CO_2^- radicals was presented in [12]. The lineshape transformation obtained in our work agrees with the results in [12]. At $T_{\rm ann} = 1000$ °C, the ratio of the amounts of orthorhombic and axial CO_2^- radicals is 0.20.

In order to analyze the variation of the total amount of CO_2^- radicals with the annealing temperature, it is convenient to use the value of $I_{\rm EPR}$ (see Fig. 1). It defines the amplitude of the EPR spectrum near the point $g = g_{||}(g_z)$. This value is proportional to the total number of orthorhombic and axial CO_2^- radicals, while no other paramagnetic centers contribute to $I_{\rm EPR}$. Moreover, $I_{\rm EPR}$ does not depend on the ratio between the amounts of axial and orthorhombic centers (within the experimental errors). The dependence of $I_{\rm EPR}$ on the annealing temperature is shown in Fig. 2. Four temperature intervals can be distinguished on this experimental curve (Fig. 2). In the first temperature interval ($T_{\rm ann} < 250$ °C), a slight increase of the intensity of the radiation-induced EPR spectrum was observed similarly to [22]. One of the explanations of this effect can be the annealing-induced decay of electron traps. These traps can capture the radiation-induced secondary electrons that participate in the formation of CO_2^- radicals. That is, the decay of traps enhances the radiation-induced signal. The nature of these traps is not known. However, it should be noted that, in the temperature interval discussed, the weakly bound water escapes from enamel, mainly, it escapes from the surface and subsurface regions of crystallites. Therefore, one can assume that the above-mentioned electron traps have the surface or subsurface origin and are related to the complexes that include water. An additional explanation of the observed increase of the amount of CO_2^- radicals can be proposed. According to [16], the annealing of tooth enamel HAP leads to a decrease of the volume of amorphous regions in HAP. It is possible that carbonate in these regions cannot be transformed into CO_2^- radicals under irradiation. The transformation of amorphous regions into the ordinary structure of HAP with CO_3^{2-} ions can increase the total number of the latter and, respectively, the amount of related CO_2^- radicals.

The second temperature interval (250–350 °C) shows the steepest decrease of the amount of CO_2^- radicals caused by the intense escape of carbonate from crystallites. This escape correlates with (and, most likely, is related to) the escape of structurally bound water from HAP [15].

A decrease of the amount of CO_2^- radicals is slowing down in the third temperature interval (350–500 °C), there is even some growth of the amount of CO_2^- radicals at $T_{\rm ann} = 400$ °C.

The fourth temperature interval (500–1000 °C) is characterized by a smooth decrease in the amount of CO_2^-.

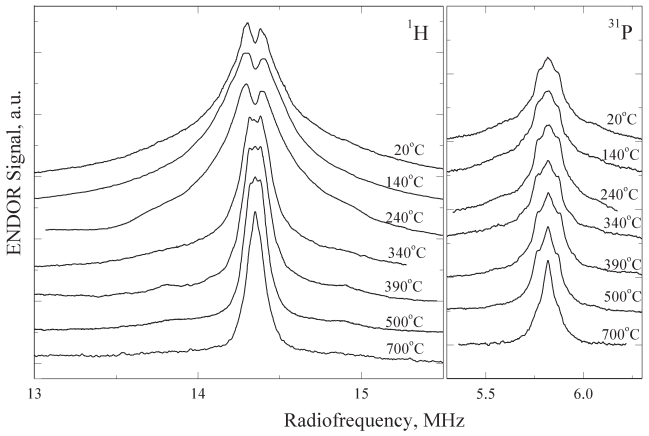

Fig. 3. Normalized ENDOR spectra of ^{1}H and ^{31}P nuclei at various annealing temperatures

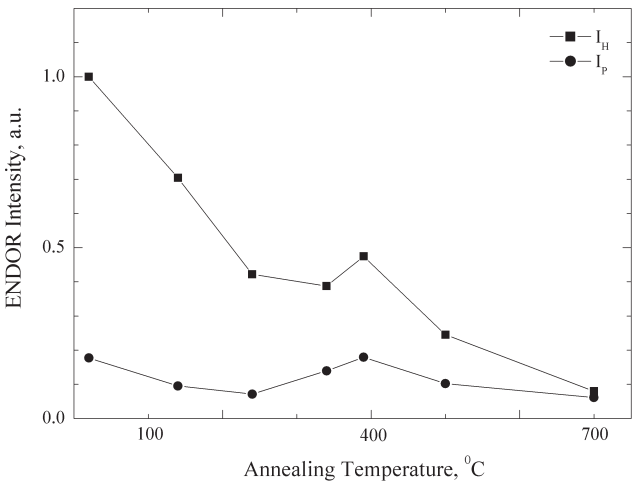

Fig. 4. Peak intensity of ^{1}H and ^{31}P ENDOR signals versus the annealing temperature

The processes at annealing temperatures of 250–1000 °C can be described as follows. Probably, the water localized in tooth enamel HAP stabilizes CO_3^{2-} ions in position B. When water leaves crystallites ($T_{ann} >$ 250 °C), CO_3^{2-} is transformed into CO_2 molecules, and the latter escape from crystallites together with water. The appearance of CO_2 molecules in the enamel structure is supported by [15], where the IR absorption peak related to CO_2 in tooth enamel was observed at $T_{ann} = 400$ °C (this peak is not observed at $T_{ann} < 200$ °C). Most probably, some CO_2 molecules that originate from CO_3^{2-} at the mentioned temperature (about 400 °C) are localized in crystallites, thus slowing down the escape of carbonate from crystallites. As a result, the possibility to form CO_2^- radicals directly from CO_2 molecules appears. This mechanism can be more efficient than the formation of CO_2^- from CO_3^{2-} and can cause the increase of the amount of radicals in the third temperature interval.

As the annealing temperature increases ($T_{ann} >$ 500 °C), no CO_2 molecules are registered [15]. Probably, their localization inside crystallites becomes impossible. On the other hand, in this temperature interval, the OH vacancies appear in crystallites. These vacancies capture CO_2 molecules that are transformed into CO_3^{2-} in position A. This process (confirmed also by IR studies [15]) causes the further decrease of the rate of carbonate escape from tooth enamel (the fourth temperature interval in Fig. 2). Note that the EPR spectra measured at $T_{ann} > 700$ °C are similar to those observed in irradiated synthetic HAP of type A [23]. This points to the thermally induced transformation of tooth enamel HAP from type B to type A.

3.2. ENDOR studies

The ENDOR spectra of protons (^{1}H) and phosphorus (^{31}P) nuclei that were observed at the EPR line maximum (near $g = g_\perp$) are shown in Fig. 3. When the external magnetic field is fixed at every point within the EPR line, the shapes and the thermally induced changes of ENDOR spectra are similar. This implies that all of them are related to the same type of paramagnetic centers, namely, to CO_2^- radicals. Figures 4 and 5 show the intensity of ENDOR lines and FWHM (full width at half maximum) versus the annealing temperature. As shown in [18], the hyperfine structure of the CO_2^- ENDOR line can be observed in biological HAP under certain conditions (in particular, under the annealing after the irradiation). This allows one to determine the hyperfine interaction constants for different nuclei surrounding CO_2^- and to define the position of CO_2^- more accurately. Under the preliminary annealing performed in the present work, the hyperfine structure of ENDOR lines was observed only at certain temperatures and was not resolved. Thus, it was impossible to carry out the analysis similar to [18]. Therefore, we have focused on the general features of ENDOR lines and changes of their intensity and width.

Proton ENDOR. The ENDOR spectra of ^{1}H nuclei in unannealed samples and ones annealed at low temperatures (see Fig. 3) are the typical matrix ENDOR spectra caused by chaotically distributed nuclei [24]. In this case, the ENDOR signal decreases with increase of the distance from a nucleus to the paramagnetic center. On the other hand, the amount of such nuclei increases that can lead to the increase of the overall signal. These

two opposite tendencies lead to the formation of two maxima of the ENDOR signal that are observed on both sides of the nuclear Larmor frequency of protons (the doublet splitting of the ENDOR line in Fig. 3).

The spatial matrix of protons surrounding CO_2^- is composed of the protons belonging both to the HAP lattice and to hydrogen-containing impurities (e.g., H_2O, OH^-). Note that, in unannealed samples and in ones annealed at low-temperature, impurity-related protons prevail. With increase of $T_{\rm ann}$, the hydrogen-containing impurities escape from crystallites. As a result, the intensity of the ENDOR signal of protons decreases, the resonance line becomes narrower, and the shape and the intensity of this line become similar to those of the phosphorus ENDOR line. The deviation from this tendency in some temperature intervals can be explained in the following way.

The intensity of the ENDOR signal is mainly determined by the EPR signal amplitude, the number of nuclei, and the relaxation processes in the spin system. The decrease of the ENDOR signal at $T_{\rm ann}$ = 20–250 °C, when the EPR signal increases (Figs. 2 and 4), indicates that the negative action of the two latter factors (the decrease of the number of nuclei and the deterioration of the relaxation conditions) dominates. The increase of the ENDOR line width in this temperature interval (Fig. 5) is caused, most probably, by the redistribution of the intensities within the spectrum in favor of the components with stronger hyperfine interaction (nuclei that are close to CO_2^-). The relative decrease of the contribution of the nuclei with weak hyperfine interaction (far nuclei) can be caused by the preferential escape of hydrogen-containing impurities from subsurface regions of crystallites. These contributions form the narrow central part of the ENDOR signal. The increase of the ENDOR line intensity near $T_{\rm ann}$ = 400 °C is caused, mainly, by the increase of the EPR signal (Fig. 2). The enhancement of the effect is possible due to more optimal relaxation conditions for the observation of ENDOR of CO_2^- centers formed from CO_2 molecules. At $T_{\rm ann} > 200$ °C, a narrow signal arises at the center of the proton ENDOR spectrum, and its relative contribution increases with the annealing temperature. At $T_{\rm ann} > 700$ °C, this signal dominates. Most likely, it is related to CO_2^- radicals in position A. A similar narrow signal of ENDOR without doublet splitting was observed in synthetic HAP of type A [23], which confirms our assumption.

Phosphorus ENDOR. Since the phosphorus-containing impurities in crystallites of HAP are absent, the ENDOR spectrum of ^{31}P nuclei is a "lattice" signal.

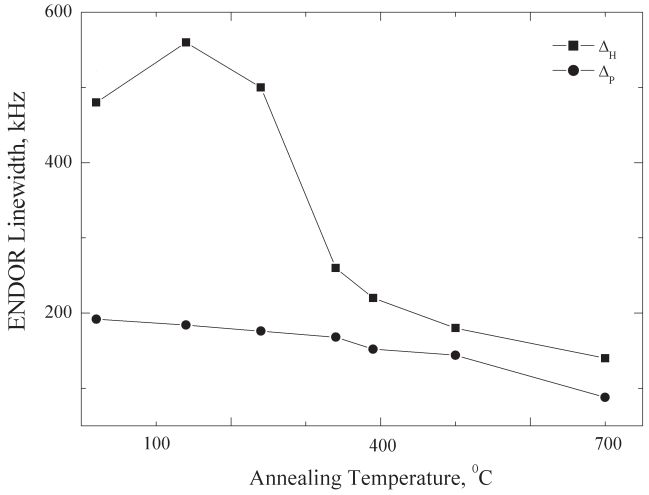

Fig. 5. Width of ENDOR signals of ^{1}H and ^{31}P nuclei versus the annealing temperature

This is corroborated by both the presence of the corresponding hyperfine structure in the spectrum and the insignificant changes of the spectrum under the annealing up to ∼500 °C (Fig. 3). The general tendency to decreasing the intensity and width of the phosphorus ENDOR line is violated only near $T_{\rm ann}$ =400 °C. Similarly to the proton signal, we ascribe this effect to specific features of the ENDOR observation from CO_2^- radicals created from CO_2 molecules. At high annealing temperatures ($T_{\rm ann} > 700$ °C), the narrow signal dominates in the central part of the phosphorus ENDOR spectrum, like in the case of proton ENDOR (Fig. 3). In our opinion, it is related to the neighboring phosphorus nuclei of CO_2^- radicals in position A.

4. Conclusion

The carbonate impurities in unannealed specimens of hydroxyapatite of tooth enamel are present mainly in the form of CO_3^{2-} carbonate-ions that substitute PO_4^{3-} ions (HAP of type B). Under irradiation, CO_3^{2-} ions are transformed into axial and orthorhombic CO_2^- radicals that can be used as probes for the study of the carbonate structure of HAP and its thermally induced changes.

Crystallites of unannealed biological HAP contain, in addition to carbonate, a great amount of hydrogen-containing impurities, structurally bound water being the dominating one. As a result, the ENDOR line of hydrogen ^{1}H nuclei is typical of the matrix ENDOR (a broad line with doublet structure). The hydrogen impurities hamper the rotation of CO_2^- radicals, and,

as a result, the orthorhombic centers dominate (∼80%) over the axial ones.

Under the annealing of HAP, the general tendency is the escape of carbonate and hydrogen-containing impurities from HAP. The former causes the decrease of the intensities of EPR and ENDOR spectra of CO_2^- radicals, while the latter causes the variation of the proton ENDOR lineshape (the transition from the "matrix" to "lattice" shape) and a relative increase in the amount of axial radicals. The phosphorus ENDOR spectrum has the form of the "lattice" ENDOR spectrum and varies slightly under annealing.

The main features of EPR and ENDOR lines are:

1. In the interval $T_{\rm ann}$ = 20–250 °C, the anomalous growth of the EPR signal is observed. This can be explained by both the annealing of traps for secondary electrons and the transformation of amorphous regions of HAP into the ordinary HAP structure with CO_3^{2-} ions that are precursors of CO_2^- radicals. Both processes cause an increase of the amount of CO_2^- radicals at a constant irradiation dose.

2. In the above-indicated temperature interval, the unusual broadening of the proton ENDOR line occurs. It is related, in our opinion, to the redistribution of the intensities within the ENDOR spectrum in favor of the components with stronger hyperfine interaction. Probably, the escape of the hydrogen-containing impurities from the crystallites starts with the escape of those species that are situated far from paramagnetic centers and form the central (narrow) part of ENDOR line.

3. Near $T_{\rm ann}$ = 400 °C, the increase of the intensity of EPR and ENDOR signals is observed. This can be explained by the appearance of localized CO_2 molecules in HAP that are also registered in IR studies [15]. The formation of CO_2^- radicals from CO_2 molecules is more efficient than that from precursors CO_3^{2-}. In this case, it can also lead to the more favorable conditions of ENDOR observation.

At high annealing temperatures ($T_{\rm ann}$ > 700 °C), the contribution of axial CO_2^- radicals dominates in the EPR spectrum of biological HAP (∼80%), the spectrum becomes similar to the EPR spectrum observed in synthetic HAP of type *A* [23]. In this case, the narrow signals, that are also characteristic of synthetic HAP of type *A*, dominate in the proton and phosphorus ENDOR spectra [23]. Therefore, one can conclude that, under the annealing, the escape of carbonate impurities occurs simultaneously with their shift from position *B* to *A*. Thus, the thermally induced transformation of biological HAP from type *B* to type *A* occurs.

1. L.G. Rozenfeld, A.B. Brik, and O.M. Atamanko, Zh. AMN Ukr. **5**, 220 (1999).
2. L.G. Rozenfeld, A.B. Brik, G.H. Kenner *et al.*, Ortop. Travm. Protez. No. 5, 9 (2002).
3. M. Ikeya, S. Miyajima, and S. Okajima, Jpn. J. Appl. Phys. **23**, L697 (1984).
4. F. Callens, Nucleonika **42**, 565 (1997).
5. G. Liidja, J. Past, J. Puskar, and E. Lippmaa, Appl. Radiat. Isot. **47**, 785 (1996).
6. D. Regulla, Appl. Radiat. Isot. **52**, 1023 (2000).
7. R. Grun, Appl. Radiat. Isot. **40**, 1045 (1989).
8. A.R. Skinner, B.A.B. Blackwell, N.D. Chasteen, J. Shao, and S.S. Min, Appl. Radiat. Isot. **52**, 1337 (2000).
9. F. Callens, P. Moens, and R. Verbeeck, Calcif. Tissue Int. **56**, 543 (1995).
10. I.P. Vorona, S.S. Ishchenko, N.P. Baran, T.L. Petrenko, and V.V. Rudko, Rad. Meas. **41**, 577 (2006).
11. I.P. Vorona, S.S. Ishchenko, M.P. Baran, and A.O. Klimov, Ukr. Fiz. Zh. **48**, 151 (2003).
12. M.P. Baran, I.P. Vorona, S.S. Ishchenko, and V.V. Rudko, Ukr. Fiz. Zh. **52**, 681 (2007).
13. T.S. Chong, T. Iida, and K. Ieda, in *Proc. of First International Symposium on ESR Dating, Japan, 1985*, p. 335.
14. H. P. Schwarcz, Nucl. Tracks. **10**, 865 (1985).
15. D.W. Holcomb and R.A. Young, Calcif. Tissue Int. **31**, 189 (1980).
16. K. Beshah, C. Rey, M.J. Glimcher, M. Schimizu, and G. Griffin, J. of Solid States Chem. **84**, 71 (1990).
17. I.P. Vorona, S.S. Ishchenko, M.P. Baran, V.V. Rudko, I.V. Zatovs'kyi, and V. Yu. Povarchuk, Ukr. Fiz. Zh. (be published).
18. S. Ishchenko, I. Vorona, and S. Okulov, Quant. Electr. & Optoelectr. **2**, 84 (1999).
19. L.G. Gilinskaya, T.N. Grigor'eva, G.N. Okuneva, and Yu.A. Vlasov, Zh. Struk. Khim. **44**, 678 (2003).
20. V.G. Grachev and Yu.G. Semenov, in *Radiospectroscopy* (Perm, 1983) (in Russian), p. 163.
21. I.P. Vorona, N.P. Baran, S.S. Ishchenko, V.V. Rudko, L.S. Chumakova, and V.Yu. Povarchuk, Fiz. Tverd. Tela **50**, 1779 (2008).
22. I.P. Vorona, S.S. Ishchenko, and N.P. Baran, Rad. Meas. **39**, 137(2005).
23. D.U. Schramm, J. Terra, A.M. Rossi, and D.E. Ellis, Phys. Rev. B **63**, 024107 (2000).
24. L. Kevan, S. Schlick, K. Torlyama, and M. Iwasaki, J. Phys. Chem. **84**, 1950 (1980).

Received 18.11.08

ТЕРМІЧНО ІНДУКОВАНІ ЗМІНИ КАРБОНАТНОЇ СТРУКТУРИ БІОЛОГІЧНОГО ГІДРОКСИЛАПАТИТУ, ДОСЛІДЖЕНІ МЕТОДАМИ ЕПР ТА ПЕЯР

С.С. Іщенко, І.П. Ворона, М.П. Баран, С.М. Окулов, В.В. Рудъко

Р е з ю м е

Методами електронного парамагнітного резонансу (ЕПР) та подвійного електронно-ядерного резонансу (ПЕЯР) досліджено зміни карбонатної структури гідроксилапатиту зубної емалі при відпалах в інтервалі температур $T_{\rm ann}$ = 20–1000 °C. В ролі зондів під час дослідження використано радикали CO_2^-, які утворювалися γ-опроміненням після відпалу зразків. Проаналізовано та пояснено вигляд і термоіндуковані зміни спектрів ЕПР та спектрів протонного (^{1}H) і фосфорного (^{31}P) ПЕЯР. Встановлено, що загальною тенденцією при відпалах біогідроксилапатиту є вихід з нього карбонатної речовини з одночасним перетворенням його при $T_{\rm ann} > 700$ °C з B-типу в A-тип. Особливості виходу карбонату з біогідроксилапатиту в діапазоні $T_{\rm ann} = 400$ °C пояснено утворенням в ньому локалізованих молекул CO_2. Одержані результати корелюють з результатами ІЧ- та ЯМР-досліджень зубної емалі та вимірами ЕПР та ПЕЯР спектрів від радикалів CO_2^- в синтетичних гідроксилапатитах.